Molecular Ladders of Lanthanide−3−phenyl−4−benzoyl−5−isoxazolonate and Bis(2−(diphenylphosphino)phenyl) Ether Oxide Complexes: The Role of the Ancillary Ligand in the Sensitizatio…

ARTICLE *in* CRYSTAL GROWTH & DESIGN · MARCH 2009

Impact Factor: 4.89 · DOI: 10.1021/cg900304g

4 AUTHORS, INCLUDING:

Biju Silvanose
University of Leuven
29 PUBLICATIONS **938** CITATIONS
SEE PROFILE

MLP Reddy
National Institute for Interdisciplinary Scie…
119 PUBLICATIONS **2,395** CITATIONS
SEE PROFILE

CRYSTAL GROWTH & DESIGN
2009
VOL. 9, NO. 8
3562–3569

Molecular Ladders of Lanthanide-3-phenyl-4-benzoyl-5-isoxazolonate and Bis(2-(diphenylphosphino)phenyl) Ether Oxide Complexes: The Role of the Ancillary Ligand in the Sensitization of Eu^{3+} and Tb^{3+} Luminescence

S. Biju,[†] M. L. P. Reddy,*[,†] Alan H. Cowley,[‡] and Kalyan V. Vasudevan[‡]

Chemical Sciences and Technology Division, National Institute for Interdisciplinary Science & Technology (NIIST), Thiruvananthapuram-695 019, India, and Department of Chemistry and Biochemistry, The University of Texas at Austin, 1 University Station A5300, Austin, Texas 78712

Received March 16, 2009; Revised Manuscript Received May 7, 2009

ABSTRACT: Three new lanthanide heterocyclic β-diketonate complexes having the general formula $Ln(PBI)_3(DPEPO)$ [HPBI = 3-phenyl-4-benzoyl-5-isoxazolone, DPEPO = bis(2-(diphenylphosphino)phenyl) ether oxide and $Ln^{3+} = Eu^{3+}$ (**1**), Tb^{3+} (**2**), and Gd^{3+} (**3**)] have been synthesized. Compounds **1** and **2** were characterized by single-crystal X-ray diffraction. The single-crystal X-ray diffraction analyses of **1** and **2** revealed that these complexes are mononuclear, and that the central Ln^{3+} ion is coordinated by six oxygen atoms furnished by three bidentate β-diketonate ligands and two oxygen atoms from the bidentate DPEPO ligand. The overall molecular geometry is distorted square prismatic. Examination of the packing diagrams for **1** and **2** revealed the presence of interesting molecular ladder structures held together by $\pi\cdots\pi$ and intermolecular hydrogen-bonding interactions. The effect of the chelating ancillary phosphine oxide ligand DPEPO on the sensitized luminescence of Eu^{3+} and Tb^{3+} luminescence in these heterocyclic β-diketonate complexes has been investigated. The ancillary ligand increases considerably the luminescence efficiency of $[Eu(PBI)_3(DPEPO)]$ (overall quantum yield 2−30%; $^5D_0$ lifetime 250−1056 μs) compared to $Eu(PBI)_3(C_2H_5OH)(H_2O)$, through the formation of intraligand states, while it is detrimental to Tb^{3+} luminescence in $[Tb(PBI)_3(DPEPO)]$ (overall quantum yield 11 to 0.5%; $^5D_4$ lifetime 400 to 168 μs).

Introduction

The fascinating optical properties of lanthanide ions have prompted the use of their coordination complexes in an increasing number of photonic applications ranging from biomedical analysis (fluoroimmunoassays, cellular imaging, and MRI contrast agents) to materials science (lasers, optical fibers, light emitting diodes).[1] Because of the Laporte forbidden character of the intra-4f transitions, luminescent lanthanide ions exhibit long-lived excited-state lifetimes and high color purity emissions that are usually insensitive to quenching by molecular oxygen, thus rendering them ideal candidates for the development of optical devices. Unfortunately, the molar absorption coefficients of lanthanide transitions are typically very small (less than 10 M^{-1} cm^{-1}). This weak absorbance can, however, be overcome by coordinating chromophore-containing ligands to the Ln^{3+} ion which, upon irradiation, transfer energy to the metal center, typically via the ligand triplet excited state, thereby populating the Ln^{3+} emitting levels in a process known as the "antenna effect".[2] The β-diketonate ligand class represents one of the important antennas for facilitating efficient ligand → Eu^{3+} and ligand → Tb^{3+} energy transfers, thus generating high harvest emissions.[2] Moreover, β-diketonates possess the additional advantage of a negatively charged binding site that results in the formation of neutral, 3:1 ligand/lanthanide luminescent complexes. β-Diketonate ligands also exhibit strong absorption over a substantial wavelength range for the $\pi-\pi^*$ transition and can therefore sensitize the lanthanide luminescence effectively. However, lanthanide β-diketonate chelates are typically isolated as mono- or dihydrates. The presence of one or two water molecules in the first coordination sphere of the central metal ion results in quenching of the emission due to the activation of nonradiative decay paths. One way to circumvent this problem is to replace the water molecules with ancillary ligands bearing chromophores that are capable of playing the antenna role. An additional requirement is that the antenna ligand binds sufficiently strongly to the lanthanide center that the coordination of water molecules is precluded. In choosing the ancillary ligand, attention should be paid to improving the volatility and thermal stability as well as the film forming properties and the carrier transport ability.

To date, the majority of lanthanide tris(β-diketonates) feature nitrogen-based antenna ligands such as 1,10-phenanthroline, 4,7-disubstituted-1,10-phenanthrolines, 2,2′-bipyridine, 4,4′-disubstituted-2,2′-bipyridines, and 2,2′:6′,6″-terpyridine, all of which have been reported to serve as efficient light conversion molecular devices.[3] By contrast, studies of the luminescent behavior of lanthanide tris-β-diketonate complexes involving triphenylphosphine oxides are much more limited.[4] Heterocyclic β-diketones such as 4-acyl-5-pyrazolones[5] and 3-phenyl-4-aryl-5-isoxazolones[6] can also be successfully employed as sensitizers for Eu^{3+} and Tb^{3+}. In particular, terbium complexes that are supported by the pyrazolone-based ligands 1-phenyl-3-methyl-4-isobutyryl-5-pyrazolone or 1-phenyl-3-methyl-4-(2-ethylbutyryl)-5-pyrazolone with triphenylphosphine oxide as the ancillary ligand have been reported to exhibit promising electroluminescence properties.[5] A highly efficient photoluminescence quantum yield of 55.3% has also been reported for a CH_2Cl_2 solution of a Eu^{3+}-2-thenoyltrifluoroacetonate complex with a phosphine oxide coligand.[7] In a previous report, we noted that Eu^{3+}-3-phenyl-4-benzoyl-5-isoxazolonates in the presence of various bidentate nitrogen coligands exhibit excellent intrinsic quantum yields.[6c] However, the overall quantum yields obtained were not very encouraging for these complexes due to the poor sensitization efficiency of the bidentate nitrogen donors. The

* To whom correspondence should be addressed. E-mail: mlpreddy55@gmail.com.
[†] National Institute for Interdisciplinary Science & Technology (NIIST).
[‡] The University of Texas at Austin.

10.1021/cg900304g CCC: $40.75
Published on Web 05/26/2009

foregoing result prompted us to synthesize three new lanthanide heterocyclic β-diketonate complexes [Eu(PBI)$_3$(DPEPO) (**1**), Tb(PBI)$_3$(DPEPO) (**2**), and Gd(PBI)$_3$(DPEPO) (**3**)] involving the 3-phenyl-4-benzoyl-5-isoxazolone (HPBI) and bis(2-(diphenylphosphino)phenyl) ether oxide (DPEPO) ligands. The role of the ancillary ligand on the sensitization process of Eu^{3+} and Tb^{3+} luminescence has been investigated. The choice of these ligands is based on their ability to coordinate strongly to lanthanide ions, their structural rigidity, and good electron-transporting properties.

Experimental Section

Materials. The following chemicals were procured commercially and used without subsequent purification: europium(III) nitrate hexahydrate, 99.9% (Acros Organics); terbium(III) nitrate hexahydrate, 99.9% (Acros Organics); gadolinium(III) nitrate hexahydrate (Treibacher); bis(2-(diphenylphosphino)phenyl)ether, 97% (Aldrich). The synthesis of the HPBI ligand was described in our previous publication.[6] All the other chemicals used were of analytical reagent grade. The precursor complexes Ln(PBI)$_3$(H$_2$O)$_2$ (Ln = Eu, Tb, Gd) were synthesized as described previously.[6]

Physical Measurements. Elemental analyses were performed with a Perkin-Elmer Series 2 Elemental Analyzer 2400. A Perkin-Elmer Spectrum One FT-IR spectrometer using KBr (neat) was used to obtain the IR spectral data and a Bruker 500 MHz NMR spectrometer was used to record the ^{1}H NMR and ^{13}C NMR spectra of DPEPO in CDCl$_3$ solution. The mass spectra were recorded on a JEOL JSM 600 fast atom bombardment (FAB) high resolution mass spectrometer (FAB-MS) and the thermogravimetric analyses were performed on a TGA-50H instrument (Shimadzu, Japan). The absorbances of the ligands were measured in CH_3CN solution on a UV−vis spectrophotometer (Shimadzu, UV-2450) and the photoluminescence (PL) spectra were recorded on a Spex-Fluorolog FL22 spectrofluorimeter equipped with a double grating 0.22 m Spex 1680 monochromator and a 450W Xe lamp as the excitation source operating in the front face mode. The lifetime measurements were carried out at room temperature using a Spex 1040 D phosphorimeter.

The overall quantum yields ($\Phi_{overall}$) were measured using an integrating sphere in a SPEX Fluorolog spectrofluorimeter. The PL quantum yields of thin films ($\Phi_{overall}$) were determined using a calibrated integrating sphere system. A Xe-arc lamp was used to excite the thin-film samples that were placed in the sphere. All samples were prepared by drop casting the material placed between two quartz coverslips. The quantum yields were determined by comparing the spectral intensities of the lamp and the sample emission as reported in the literature.[8] Using this experimental setup and the integrating sphere system, the solid-state fluorescence quantum yield of a thin film of the standard green OLED material tris-8-hydroxyquinolinolato aluminum (Alq_3) was determined to be 0.19, which is consistent with previously reported values.[9] Each sample was measured several times under slightly different experimental conditions. The estimated error for the quantum yields is ($\pm$10%).[10]

Synthesis of Bis(2-(diphenylphosphino)phenyl) Ether Oxides (DPEPO). DPEPO was synthesized according to the method described by Xu et al.[7] (Scheme 1). One milliliter of 30% H_2O_2 (10.5 mmol) was added dropwise to a vigorously stirred solution of 5 mmol of bis(2-(diphenylphosphino)phenyl) ether in 10 mL of 1,4-dioxane. The resulting reaction mixture was stirred for 2 h, following which the reaction was quenched. The reaction mixture was then extracted with 3 × 30 mL portions of dichloromethane. The resulting oily phase was next washed with 2 × 30 mL portions of water to remove 1,4-dioxane and the dichloromethane layer was dried with Na_2SO_4. Following solvent removal in vacuo, DPEPO was isolated as a white powder in a yield of 99%. ^{1}H NMR (500 MHz, CDCl$_3$, TMS): δ (ppm) 7.709−7.622 (m, 9H, Phen-H); 7.487−7.266 (m, 13H, Phen-H); 7.172−7.139 (tr, 2H, Phen-H); 7.079 (tr, 2H, Phen-H); 7.096 (q, 2H,) 5.29. ^{13}C NMR (500 MHz, CDCl$_3$, TMS): δ (ppm) 134.10−124.48, 123.77, 120.12, 77.28−76.77 (CDCl$_3$). IR (KBr) λ_{max}: 1590, 1566, 1461, 1435, 1221, 1197, 1120, 1074, 877, 804, 748, 707, 549 cm^{-1}. m/z = 571.60 (M + 1).

Synthesis of Complexes 1−3. Complexes **1**−**3** were prepared by stirring equimolar solutions of Ln(PBI)$_3$(H$_2$O)$_2$ and DPEPO in CHCl$_3$ solution for 24 h at 70 °C (Scheme 2). The products were isolated by solvent evaporation and purified by recrystallization from a chloroform−hexane mixture. Crystals suitable for single-crystal X-ray diffraction experiments were obtained from saturated solutions of the complexes in 2-methoxy-ethanol stored at ambient temperature over a period of six months.

Scheme 1. Synthesis of the DPEPO Ligand

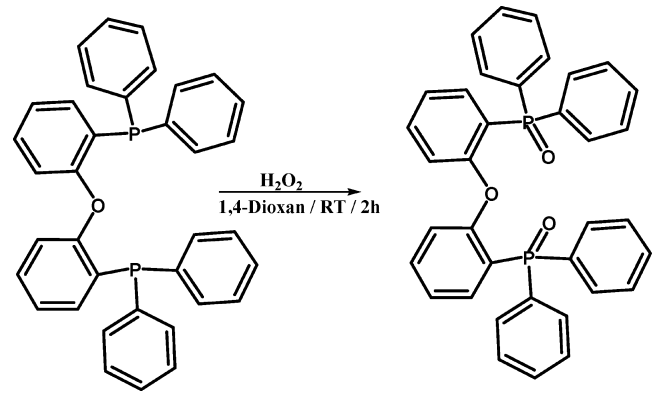

Eu(PBI)$_3$(DPEPO) (1). Elemental analysis (%): calcd for $C_{84}H_{58}EuN_3O_{12}P_2$ (1515.28): C, 66.58; H, 3.86; N, 2.77. Found: C, 66.61; H, 3.96; N, 2.79. IR (KBr) λ_{max}: 1652, 1480, 1435, 1385, 1229, 1180, 1118, 1072, 903, 781, 760, 698, 544 cm^{-1}; m/z = 1252.03 [Eu(PBI)$_2$(DPEPO)] + 1.

Tb(PBI)$_3$(DPEPO) (2). Elemental analysis (%): calcd for $C_{84}H_{58}TbN_3O_{12}P_2$ (1522.25): C, 66.28; H, 3.84; N, 2.76. Found: C, 66.31; H, 3.95; N, 2.78. IR (KBr) λ_{max}: 1652, 1495, 1480, 1436, 1389, 1224, 1180, 1181, 1118, 1073, 905, 758, 693, 546 cm^{-1}; m/z = 1259.01 [Tb(PBI)$_2$(DPEPO)] + 1.

Gd(PBI)$_3$(DPEPO) (3). Elemental analysis (%): calcd for $C_{84}H_{58}GdN_3O_{12}P_2$ (1520.57): C, 66.35; H, 3.84; N, 2.76. Found: C, 66.41; H, 4.00; N, 2.85. IR (KBr) λmax: 1651, 1480, 1436, 1386, 1230, 1181, 1122, 1071, 904, 758, 694, 547 cm^{-1}; m/z = 1257.31 [Gd(PBI)$_2$(DPEPO)] + 1.

Synthesis of Gd(DPEPO)(NO$_3$)$_3$. One mmole of Gd(NO$_3$)$_3$(H$_2$O)$_6$ (dissolved in 0.1 mL of water) was added dropwise to a stirred ethanolic solution of DPEPO (1 mmol), and the reaction mixture was refluxed for 2 h at 70 °C. The resulting white precipitate was filtered and recrystallized from a chloroform−hexane mixture. Elemental analysis (%): calcd for $C_{36}H_{28}GdN_3O_{12}P_2$ (913.82): C, 47.32; H, 3.09; N, 4.60. Found: C, 47.44; H, 3.16; N, 4.69. IR (KBr) λ_{max}: 1588, 1565, 1461, 1436, 1386, 1308, 1234, 1155, 1135, 1111, 879, 722, 717, 693, 550, 514 cm^{-1}; m/z = 852.90 [Gd(DPEPO)(NO$_3$)$_2$] + 1.

X-ray Crystallographic Characterization of 1 and 2. The X-ray diffraction data were collected at 153 K on a Nonius Kappa CCD diffractometer equipped with an Oxford Cryostream low-temperature device and a graphite-monochromated Mo Kα radiation source (λ = 0.71073 Å). Corrections were applied for Lorentz and polarization effects. Both structures were solved by direct methods[11] and refined by full-matrix least-squares cycles on F^2. All of the non-hydrogen atoms were allowed anisotropic thermal motion, and the hydrogen atoms were placed in fixed, calculated positions using a riding model (C−H, 0.96 Å).

X-ray crystallographic information files can be obtained free of charge via www.ccdc.cam.ac.uk/consts/retrieving.html (or from CCDC, 12 Union Road, Cambridge CB2 1EZ, U.K.; fax +44 1223 336033; e-mail deposit@ccdc.cam.ac.uk). CCDC numbers: 714823 for **1** and 702913 for **2**.

Results and Discussion

Spectroscopic Characterization of Ln^{3+} Complexes. The synthetic procedures for the Ln^{3+} complexes **1**−**3** are illustrated in Scheme 2. The microanalysis and HRMS data for **1**−**3** imply that Ln^{3+} ion has reacted with HPBI in a metal-to-ligand mole ratio of 1:3 and that one molecule of DPEPO is also involved in the coordination sphere. The IR carbonyl stretching frequency of the ligand HPBI (1699 cm^{-1}) is shifted to lower wave

Scheme 2. Synthesis of Complexes 1−3

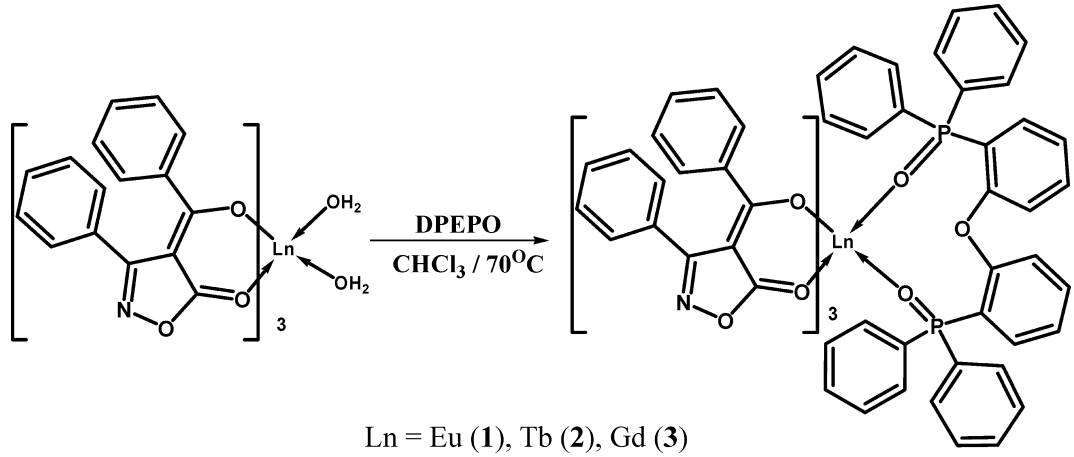

Ln = Eu (**1**), Tb (**2**), Gd (**3**)

numbers in **1**−**3** (1652 cm^{-1} in **1**; 1652 cm^{-1} in **2**; 1651 cm^{-1} in **3**), thus indicating the coordination of the carbonyl oxygen to the Ln^{3+} cation in each case.[6] Furthermore, the red shifts observed in the P═O stretching frequency of DPEPO (1197 cm^{-1}) in complexes **1**−**3** (decreased to 1180 cm^{-1} in **1** and **2** and 1181 cm^{-1} in **3**) confirm the coordination of DPEPO to each of the Ln^{3+} ions. The thermal behavior of the new Ln^{3+} complexes was examined by means of thermogravimetric analysis (TGA) under a nitrogen atmosphere. The general profile of weight loss is similar for each of the three complexes (Figure S1, Supporting Information). Thermogravimetric analysis showed that the thermal decomposition temperatures (T_d) of complexes **1**−**3** are higher than 250 °C. Subsequent thermal decomposition of **1**−**3** takes place in the region of 300−800 °C and consists of two steps. For each complex, the residue comprises approximately 12% of the initial mass and corresponds to the formation of the respective lanthanide oxide in each case. The DSC curves for complexes **1**−**3** exhibit broad endothermic peaks in the temperature range 250 to 300 °C relative to the decomposition of these complexes, as observed in the first event of the TG curve (Figure S2, Supporting Information).

X-ray Structural Characterization. The single-crystal X-ray structures of complexes **1**−**2** were determined and the molecular structures are depicted in Figures 1 and S3 (in Supporting Information), respectively. The crystal data and the data collection parameters are presented in Table 1, and selected bond lengths and bond angles are listed in Table 2. Both compounds were isostructural and crystallize in the triclinic space group $P\bar{1}$. The single crystal X-ray data indicate that complexes **1** and **2** are devoid of an inversion center; hence there is an increase in the number of electronic transitions of the 4f orbitals due to the odd parity.[4] In each case, the Ln^{3+} ion is surrounded by eight oxygen atoms, six of which are furnished by the three bidentate heterocyclic β-diketonates, and the remaining two oxygen atoms stem from the chelating phosphine oxide DPEPO

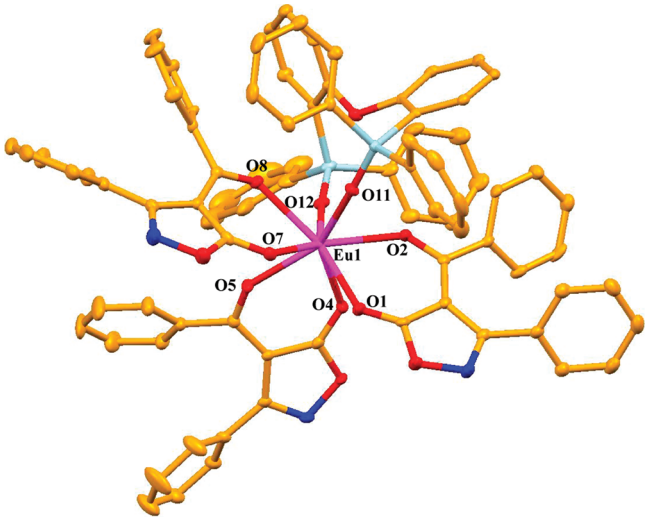

Figure 1. Asymmetric unit of complex **1**. Thermal ellipsoids are shown at the 30% probability level and all hydrogen atoms have been omitted for clarity.

Table 1. Crystallographic and Refinement Data for 1 and 2

	1	**2**
chemical formula	$C_{84}H_{58}EuN_3O_{12}P_2$	$C_{84}H_{58}TbN_3O_{12}P_2$
M	1515.23	1522.27
crystal system	triclinic	triclinic
space group	$P\bar{1}$	$P\bar{1}$
cryst size/mm^3	0.14× 0.12 × 0.09	0.20 × 0.16 × 0.11
Temp/K	153(2)	153(2)
a/(Å)	12.383(3)	12.377(3)
b/(Å)	12.839(3)	12.833(3)
c/(Å)	23.534(4)	23.510(5)
α (deg)	100.62(3)	100.58(3)
β (deg)	95.73(3)	95.75(3)
γ (deg)	107.39(3)	107.52(3)
V/$Å^3$	3461.3(12)	3451.8(12)
Z	2	2
D/(Mg m^{-3})	1.454	1.465
μ/(mm^{-1})	1.021	1.140
F(000)	1544	1548
*R*1 [$I > 2\sigma(I)$]	0.0514	0.0640
*wR*2 [$I > 2\sigma(I)$]	0.0861	0.1157
*R*1 (all data)	0.1	0.1151
*wR*2 (all data)	0.0993	0.1346
GOF	1.035	1.030

Table 2. Selected Bond Lengths (Å) and Angles (°) for 1 and 2

1		**2**	
Eu(1)−O(1)	2.392(3)	Tb(1)−O(1)	2.364(3)
Eu(1)−O(2)	2.394(3)	Tb(1)−O(2)	2.372(3)
Eu(1)−O(4)	2.469(3)	Tb(1)−O(4)	2.449(3)
Eu(1)−O(5)	2.382(2)	Tb(1)−O(5)	2.359(3)
Eu(1)−O(7)	2.432(3)	Tb(1)−O(7)	2.411(3)
Eu(1)−O(8)	2.413(3)	Tb(1)−O(8)	2.394(3)
Eu(1)−O(11)	2.328(3)	Tb(1)−O(11)	2.303(3)
Eu(1)−O(12)	2.308(3)	Tb(1)−O(12)	2.288(3)
O(1)−Eu(1)−O(2)	73.57(9)	O(1)−Tb(1)−O(2)	74.25(11)
O(4)−Eu(1)−O(5)	71.19(9)	O(4)−Tb(1)−O(5)	71.54(10)
O(7)−Eu(1)−O(8)	71.75(9)	O(7)−Tb(1)−O(8)	72.49(11)
O(11)−Eu(1)−O(12)	105.63(9)	O(11)−Tb(1)−O(12)	105.92(11)

Table 3. Distances (Å) and Angles (°) of Hydrogen Bonds for Compounds 1−2

complex	contact type	H···A (Å)	D···A (Å)	D−H···A (°)
1	C59−H59···O9	2.57	3.20	125
	C60−H60···N3	2.69	3.42	136
	C47−H47···N2	2.68	3.40	134
	C82−H82···O7	2.50	3.39	160
2	C59−H59···O9	2.57	3.20	126
	C60−H60···N3	2.72	3.44	135
	C47−H47···N2	2.69	3.40	133
	C82−H82···O7	2.50	3.39	160

ligand. The coordination polyhedra are of approximate C_{2v} symmetry and can best be described as distorted square antiprisms. Interestingly, the bridging oxygen atom connecting the two triphenyl phosphine oxide units of the DPEPO ligand is not coordinated to the central Ln^{3+} ion in either of the complexes. The two Ln−O bonds to the DPEPO ligand (2.33 Å and 2.31 Å for **1;** 2.30 Å and 2.29 Å for **2**) are shorter than the six Ln−O bonds to the HPBI ligands (2.38−2.47 Å for **1**; 2.36−2.45 Å for **2**). A similar trend of bond distances has been observed for the complexes, tris(deuterated hexafluoroacetylaceto)europium(III)-triphenyl phosphine oxide (TPPO)[4] (the Eu−O bond distances are 2.31−2.32 Å for the TPPO ligand and 2.39−2.44 Å for the β-diketonate). In the case of tris(1-phenyl-3-methyl-4-*tert*-butylacetyl-5-pyrazolonato)terbium(III)-triphenyl phosphine oxide[5d] the Tb−O bond distances are 2.30 Å for the TPPO ligand and 2.28−2.40 Å for the β-diketonates. It is also noteworthy that the Ln−O bond distances for the DPEPO ligand are shorter than those for TPPO.

Intermolecular Hydrogen Bonds and $\pi\cdots\pi$ Stacking Interactions. It was repeatedly made clear that the C−H···O/N hydrogen bonds play an important role in determining the crystal packing and to some degree the molecular conformation.[12] Scrutiny of the packing diagram for **1** revealed two types of intermolecular hydrogen bonding interactions, namely, between C59−H59···O9 and C60−H60···N3 for which the H···O/N distances are 2.57 and 2.69 Å, and the C−H···O/N angles are 125 and 136°, respectively.[13,14] Distances (Å) and angles (°) of hydrogen bonds for complexes **1**−**2** are given in Table 3. Similarly, in the case of **2**, two types of intermolecular hydrogen bonding interactions are evident between C59−H59···O9 and C60−H60···N3, with H···O/N distances of 2.57 and 2.72 Å and C−H···O/N angles of 126 and 135°, respectively. These two types of intermolecular hydrogen bonding interaction combine to generate an interesting infinite one-dimensional (1D) molecular array along the *c* axis of both **1** and **2**. The existence of C−H···O/N hydrogen bonds of this type is well-known.[14−16] Aromatic−aromatic or $\pi\cdots\pi$ interactions are important non-covalent intermolecular forces similar to hydrogen bonding. They can contribute to self-assembly or molecular recognition processes when extended structures are formed from building blocks with aromatic moieties.[17] In the cases of **1** and **2** strong intermolecular $\pi\cdots\pi$ stacking interactions are evident between the phenyl rings of the HPBI moieties (C4−C9) with an average interplanar distance of 3.52 Å.[17] Both of these van der Waals interactions (intermolecular hydrogen bonding and $\pi\cdots\pi$ stacking interactions) combine to produce a infinite 1D molecular ladder which is aligned along the *c* axis (Figures 2 and S4). The infinite 1D molecular array comprises two types of intermolecular interactions, namely, hydrogen bonds which form the strands and intermolecular $\pi\cdots\pi$ stacking interactions which connect the two 1D strands, thereby forming the steps of the molecular ladder.

Further examination of the solid-state structure of **1** revealed the presence of another array that oriented along the *a* axis.

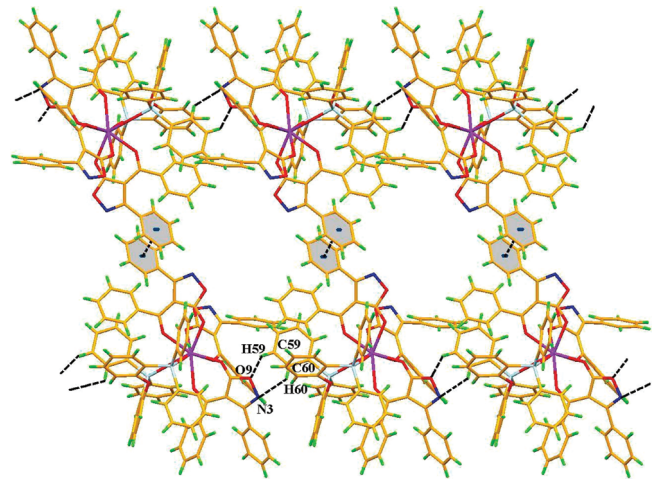

Figure 2. Molecular ladder of complex **1** involving $\pi\cdots\pi$ interactions (C4−C9) and intermolecular hydrogen bonding interactions (C59−H59···O9, C60−H60···N3), when viewed along the direction of the *c* axis.

This 1D array is illustrated by the intermolecular hydrogen bonding interaction between C47 and N2 through H47 with a H···N distances of 2.68 Å, and a C−H···N angle of 134°. In the case of **2**, the infinite 1D array is formed by intermolecular hydrogen bonding interactions C47 and N2 through H47 with a H···N distance of 2.69 Å and a C−H···N angle of 133°. Furthermore, a moderate intermolecular $\pi\cdots\pi$ stacking interaction is evident between the phenyl rings of the DPEPO units, the average interplanar distances for which are 3.84 Å for both **1** and **2.** These moderate intermolecular $\pi\cdots\pi$ stacking interaction are supplemented by intermolecular hydrogen bonding interactions between C82−H82···O7 with a H···O distance of 2.50 Å and a C82−H82···O7 angle of 160° in the case of **1**. In the case of **2**, the H82···O7 distance is 2.50 Å and the C82−H82···O7 angle is 160°. In turn, these van der Waals interactions (intermolecular hydrogen bonding and $\pi\cdots\pi$ stacking interaction) create another interesting infinite molecular ladder in the direction of *a* axis (Figures 3 and S5). The two infinite molecular ladders which extend along the directions of *a* and *c* axes combine to form a two-dimensional net-like molecular arrangement.

Solid State Luminescent Properties of 1 and 2. The excitation spectrum of the Eu^{3+} complex **1**, which was recorded at 298 K and monitored around the intense $^5D_0 \rightarrow {}^7F_2$ transition of the Eu^{3+} cation, is shown in Figure 4. The excitation spectrum of $Eu(PBI)_3(C_2H_5OH)(H_2O)$ is provided as an inset to Figure 4 for purposes of comparison. The excitation spectra recorded for the metal-centered emission of the Eu^{3+}complex in the solid state overlaps the absorption spectra of the ligands (HPBI and DPEPO) in the region 250−400 nm, thus indicating that the ligand-to-Eu^{3+} energy transfer proceeds through the triplet state (Figure S6, Supporting Information). A series of sharp lines which are assigned to transitions between the $^7F_{0,1}$ and $^5L_6$,$^5D_{3-1}$ levels are also evident in the excitation spectra of these complexes. However, these transitions are weaker than the absorptions due to the organic ligands and are overlapped by a broad excitation band, thus proving that luminescence sensitization that arises from excitation of the ligand is considerably more efficient than the direct excitation of the Eu^{3+} absorption level. The contributions from the excited states of HPBI and DPEPO toward the Eu^{3+} centered luminescence in **1** are proved by the complete overlap between the excitation spectra of the Gd^{3+}complex **3** and the Eu^{3+}complex **1** (Figure S7, Supporting

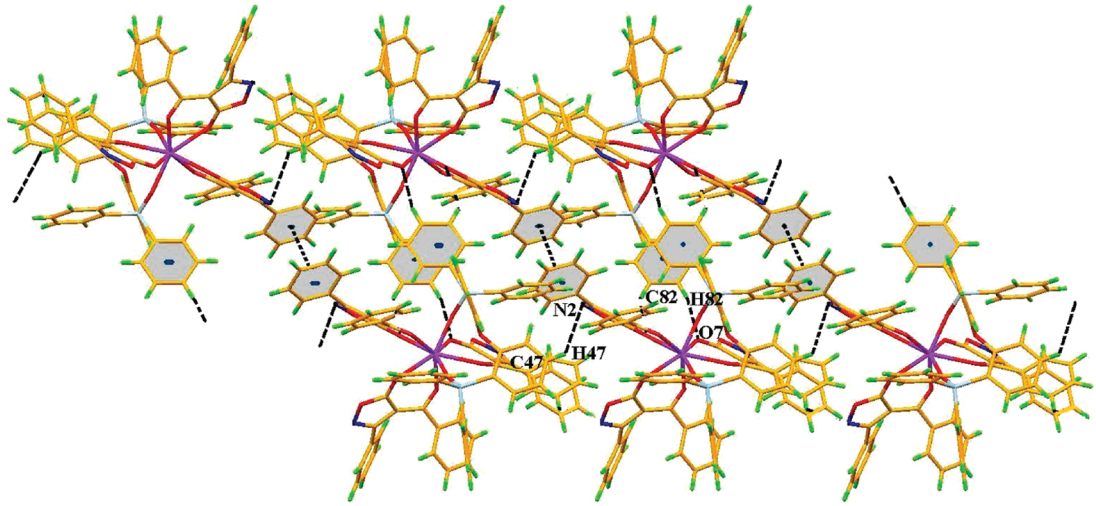

Figure 3. Molecular ladder of complex **1** involving $\pi\cdots\pi$ interactions (C4−C9, C79−C84) and intermolecular hydrogen bonding interactions (C47−H47···N2, C82−H82···O7), when viewed along the direction of the *a* axis.

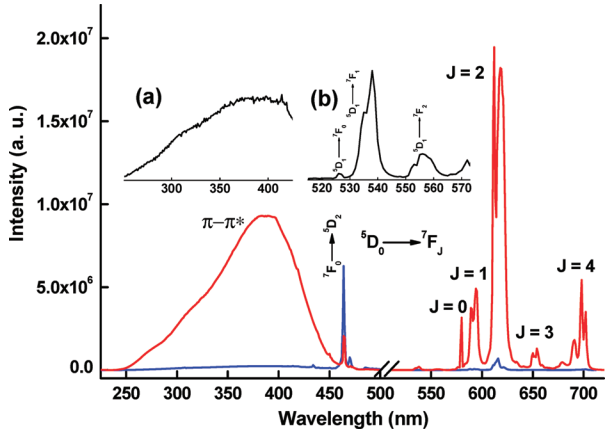

Figure 4. Solid-state excitation and emission spectra for complexes **1** (red line; λ_{ex} 390 nm) and **[**$Eu(PBI)_3(C_2H_5OH)(H_2O)$] (blue line; λ_{ex} 360 nm) at 298 K with emission monitored around 612 nm. (a) Excitation spectrum for $[Eu(PBI)_3(C_2H_5OH)(H_2O)]$, (b) $^5D_1 \rightarrow {}^7F_{0-1}$ transitions for **1**.

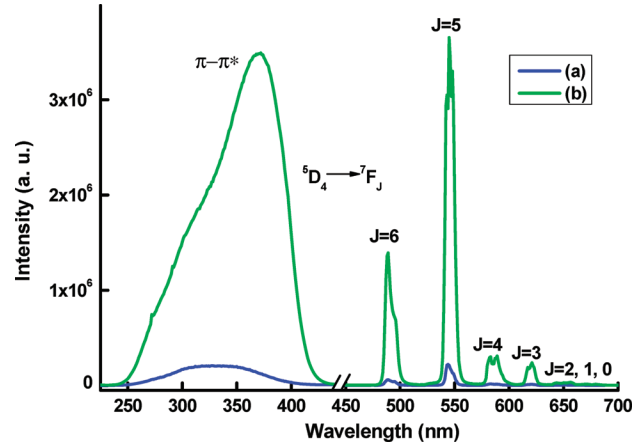

Figure 5. Solid-state excitation and emission spectra for complexes **2** (a; λ_{ex} 330 nm) and $[Tb(PBI)_3(H_2O)_2]$ (b; λ_{ex} 370 nm) at 298 K with emission monitored around 545 nm.

Information). Because of the extended conjugation induced by the $\pi\cdots\pi$ stacking interactions in the case of **1**, the excitation wavelength extends into the visible region, which helps to sensitize the Eu^{3+} emission in the visible excitation region.

Complex **1** exhibits the characteristically intense transitions of the Eu^{3+} ion upon excitation at 390 nm. As shown in Figure 4, the transitions from the excited $^5D_0$ state to the different *J* levels of the lower ^7F state were observed in the emission spectrum that was recorded at room temperature ($J = 0-4$), that is, $^5D_0 \rightarrow {}^7F_0$ at 579 nm, $^5D_0 \rightarrow {}^7F_1$ at 594 nm, $^5D_0 \rightarrow {}^7F_2$ at 612 nm, $^5D_0 \rightarrow {}^7F_3$ at 654 nm, and $^5D_0 \rightarrow {}^7F_4$ at 698 nm.[3c,6a−c,18] Furthermore, the transitions from the excited $^5D_1$ state to the $^7F_{0-1}$ state (536 nm, 556 nm) were also evident.[19] The transition of highest intensity is dominated by the hypersensitive $^5D_0 \rightarrow {}^7F_2$ transition which occurs around 612 nm, thus indicating that the rare earth ion is not located in a site with inversion center symmetry. Moreover, the presence of only one sharp peak in the region of the $^5D_0 \rightarrow {}^7F_0$ transition at 579 nm suggests the existence of a single chemical environment around the Eu^{3+} ion of point group symmetry *Cs*, *Cn*, or *Cnv*,[2c,5a−c,20] which is in good agreement with the X-ray crystal structure of **1**. It is clear from the Figure 4 that the displacement of the solvent molecules from the complex $Eu(PBI)_3(C_2H_5OH)(H_2O)$ by the chelating phosphine oxide DPEPO significantly enhances the luminescent intensity.

The steady-state excitation and emission spectra of $Tb(PBI)_3(H_2O)_2$ and **2** in the solid state at room temperature are shown in Figure 5. The excitation spectrum of the Tb^{3+} complex **2** monitored around the peak of the intense $^5D_4 \rightarrow {}^7F_5$ transition of the Tb^{3+} ion exhibits a broadband between 250 and 400 nm with a maximum at approximately 330 nm, which can be assigned to the $^1\pi-\pi^*$ electronic transition of the DPEPO ligand. On the other hand, $Tb(PBI)_3(H_2O)_2$ exhibits a broadband with an excitation maximum at 370 nm, due to the $^1\pi-\pi^*$ electronic transition of the HPBI ligand. Furthermore, it is evident from Figure S8, Supporting Information that the contribution from the excited states of DPEPO toward the Tb^{3+} centered luminescence in the case of **2** is much higher than that from the β-diketonate ligand HPBI (Note that there is partial overlapping between the excitation spectra of **2** and **3**). The absence of any absorption bands due to the f−f transitions of the Tb^{3+} cation proves that luminescence sensitization via excitation of the ligand is more effective than the direct excitation of the Tb^{3+} ion.

The replacement of water molecules of $Tb(PBI)_3(H_2O)_2$ by the DPEPO ligand results in a dramatic decrease in luminescence

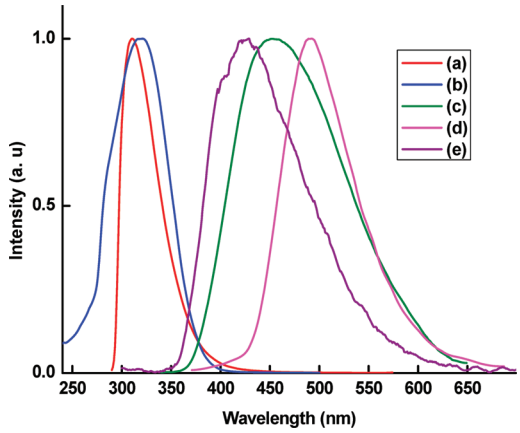

Figure 6. Room-temperature emission spectrum of DPEPO (a), UV−vis absorption spectra of HPBI (b), room-temperature emission spectrum of HPBI (c), 77 K phosphorescence spectra of $Gd(PBI)_3(H_2O)_2$ (d), 77 K phosphorescence spectra of $Gd(DPEPO)(NO_3)_3$ (e); the complexes and ligands are at 2×10^{-5} M in CH_3CN. All spectra are normalized to a constant intensity at the maximum.

intensity as can be seen in Figure 5. The room-temperature emission spectra of the Tb^{3+} complexes excited at their maximum excitation wavelengths ($\lambda_{ex} = 330$ nm for **2** and 370 nm for $Tb(PBI)_3(H_2O)_2$) exhibit the characteristic emission bands for Tb^{3+}-centered emission at 490, 545, 585, and 620 nm, which result from deactivation of the $^5D_4$ excited state to the corresponding ground state ^7F_J ($J = 6, 5, 4, 3$) of the Tb^{3+} ion. The most intense emission is centered at 545 nm and corresponds to the $^5D_4 \rightarrow {}^7F_5$ transition.[5c,d,6d] No emission bands from the HPBI or DPEPO ligands are observed in these complexes, thus implying efficient energy transfer from these ligands to the central Tb^{3+} ion.

In addition to the steady-state emission spectra of complexes **1** and **2**, the luminescent lifetimes of these complexes were measured at both room temperature (298 K) and low temperature (77 K) from the respective luminescent decay profiles by fitting with monoexponential decay curves (Figures S9−S11, Supporting Information). Collectively, these data indicate the existence of a single chemical environment around the Ln^{3+} ion in each case. The pertinent values are summarized in Table 4.

The overall quantum yield ($\Phi_{overall}$) for a lanthanide complex treats the system as a "black box" in which the internal process is not considered explicitly. Given that the complex absorbs a photon (i.e., the antenna is excited), the overall quantum yield can be defined as follows:[21]

$$\phi_{overall} = \phi_{sen} \times \phi_{ln} \quad (1)$$

Here, Φ_{sen} represents the efficiency of energy transfer from the ligand to the Ln^{3+} ion and Φ_{Ln} represents the intrinsic quantum yield of the Ln^{3+} ion, which can be calculated as

$$\phi_{Ln} = \left(\frac{A_{RAD}}{A_{RAD} + A_{NR}}\right) = \frac{\tau_{obs}}{\tau_{RAD}} \quad (2)$$

For the Eu^{3+} complex **1**, the radiative lifetime (τ_{RAD}) can be calculated using eq 3,[22,6a−c] assuming that the energy of the $^5D_0 \rightarrow {}^7F_1$ transition (MD) and its oscillator strength are constant

$$A_{RAD} = \frac{1}{\tau_{RAD}} = A_{MD,0} n^3 \left(\frac{I_{TOT}}{I_{MD}}\right) \quad (3)$$

where $A_{MD,0}$ (14.65 s^{-1}) is the spontaneous emission probability of the $^5D_0 \rightarrow {}^7F_1$ transition in vacuo, I_{TOT}/I_{MD} is the ratio of the total area of the corrected Eu^{3+} emission spectrum to the area of the $^5D_0 \rightarrow {}^7F_1$ band, and n is the refractive index of the medium. An average index of refraction equal to 1.5 was employed.[6a] The intrinsic quantum yield for Tb^{3+} (Φ_{Tb}) was estimated using eq 4 with the assumption that the decay process at 77 K in a deuterated solvent is purely radiative.[23]

$$\phi_{Tb} = \frac{\tau_{obs(298K)}}{\tau_{RAD(77K)}} \quad (4)$$

The overall quantum yield ($\Phi_{overall}$), radiative (A_{RAD}), and nonradiative (A_{NR}) decay rates, intrinsic quantum yield (Φ_{Ln}) and energy transfer efficiency (Φ_{sen}) for complexes **1** and **2** are presented in Table 4. In the solid state, the overall quantum yields for these complexes were determined according to the absolute method of Wrighton et al.[24] At room-temperature, the substitution of solvent molecules in the Eu^{3+}-tris(3-phenyl-4-benzoyl-5-isoxazolonate) complex by the chelating phosphine oxide, DPEPO leads to a 4-fold increase in the $^5D_0$ luminescence lifetime and an approximately 15-fold enhancement in the absolute quantum yield. The substantial contribution of the chelating phosphine oxide to the overall sensitization of the Eu^{3+}-centered luminescence in **1** is confirmed by (i) an increase of the intrinsic quantum yield by a factor of 2.3 which results from removal of the quenching effect of the O−H vibrations, and (ii) the significant enhancement of $\Phi_{sen.}$ from 8 to 45%. Furthermore, due to the extended conjugation induced by the $\pi\cdots\pi$ stacking interactions, complex **1** also exhibits visible light sensitized red luminescence with $\Phi_{overall} = 8 \pm 1\%$ at 410 nm and $4 \pm 0.4\%$ at 430 nm. It is evident from Table 4 that the overall quantum yield and sensitization efficiency has been enhanced significantly in the presence of bidentate phosphine oxide as the ancillary ligand than that of bidentate nitrogen donor in Eu^{3+}-tris(3-phenyl-4-benzoyl-5-isoxazolonate) complexes.[6c]

By contrast, the displacement of water molecules in $Tb(PBI)_3(H_2O)_2$ by the chelating phosphine oxide, DPEPO is detrimental to the luminescent properties. Both the room-temperature $^5D_4$ lifetime and the quantum yield decreased dramatically. This is due to the overlap of the low energy ligand centered states with the Tb^{3+} excited states which allows back energy transfer (Figure S12, Supporting Information). This view is confirmed by the fact that $^5D_4$ lifetime increases to 939 μs at 77 K from 168 μs at 298 K. The lifetime of complex **2** is higher than that of $Tb(PBI)_3(H_2O)_2$ at 77 K, and hence it can be concluded that, although the presence of the ancillary ligand reduced the O−H quenching effect by eliminating the water molecules from the first coordination sphere, it still contributes substantially to the back energy transfer process. The intrinsic quantum yield and sensitization efficiency for **2** is also significantly decreased in comparison with that of $Tb(PBI)_3(H_2O)_2$. Similar results have been noted recently in the Tb^{3+}-β-diketonate-*N,N*-dimethylaminoethanol complexes.[10]

It is well documented in previous luminescence studies of trivalent lanthanide chelates that the general mechanism for the sensitization of Ln^{3+} ion luminescence via the "antenna effect" involves the following steps: (i) UV absorption of the organic chromophore which results in excitation to the first excited singlet state; (ii) nonradiative intersystem crossing from the singlet to the triplet state; (iii) intramolecular energy transfer from the ligand-centered triplet state to the excited 4f states of the Ln^{3+} ion; and (iv) radiative transition from the Ln^{3+} ion emissive states to lower energy states which results in the

Table 4. Radiative (A_{RAD}) and Nonradiative (A_{NR}) Decay Rates, $^5D_0/^5D_4$ Lifetimes (τ_{obs}), Intrinsic Quantum Yields (Φ_{Ln}), Energy Transfer Efficiencies (Φ_{senc}), and Overall Quantum Yields ($\Phi_{overall}$) for 1 and 2

complex	A_{RAD} (s^{-1})	A_{NR} (s^{-1})	τ_{77K} (μs)	τ_{obs} (μs)	Φ_{Ln} (%)	Φ_{sen} (%)	$\Phi_{overall}$ (%)
$Eu(PBI)_3(DPEPO)$ (**1**)	556	387		1060 ± 5	59	45	30 ± 3
$Eu(PBI)_3(EtOH)(H_2O)$[6c]	1059	2941		250 ± 3	26	8	2 ± 0.2
$Eu(PBI)_3(phen)$[6c]	554	421		1025 ± 5	57	20	11 ± 1
$Tb(PBI)_3(DPEPO)$ (**2**)			939 ± 5	168 ± 1	18	3	0.5 ± 0.05
$Tb(PBI)_3(H_2O)_2$[6d]			809 ± 2	400 ± 1	49	22	11 ± 1

characteristic lanthanide emission.[2] Thus, the intramolecular energy migration efficiency from the organic ligands to the central Ln^{3+} is the most important factor determining the luminescence properties of lanthanide complexes.[2] The shortest-wavelength phosphorescence band in the phosphorescence spectrum of the $Gd(NO_3)_3(DPEPO)$ at 77K (Figure 6) was assumed to be the 0−0 transition,[2c,6d] from which the energy of the lowest triplet state, T_1 ($^3\pi\pi^* = 25640\ cm^{-1}$) was determined. The T_1 state of the HPBI ligand ($^3\pi\pi^* = 22220\ cm^{-1}$) was taken from our previous report.[6d] The singlet energy levels of DPEPO ($^1\pi\pi^* = 32260\ cm^{-1}$) and HPBI ($^1\pi\pi^* = 27640\ cm^{-1}$) were estimated from the higher absorption edges of the corresponding absorption spectra of the Gd^{3+} analogues. The triplet levels of DPEPO and HPBI were found to be higher in energy than the $^5D_{0-2}$ state of Eu^{3+}. Furthermore, these energy gaps are too large to allow back energy transfer.[25] As a consequence, these ligands can transfer energy effectively to the emitting states of the Eu^{3+} ion. On the other hand, in the case of Tb^{3+}, the energy gap between the triplet energy level of the HPBI ligand and the $^5D_4$ emitting level occurs at 1820 cm^{-1} thereby facilitating the back energy transfer process.[25] According to Reinhoudt's empirical rule,[26] the intersystem crossing process becomes effective when $\Delta E(^1\pi\pi^* - ^3\pi\pi^*)$ is at least 5000 cm^{-1}. The $\Delta E(^1\pi\pi^* - ^3\pi\pi^*)$ energy gaps for DPEPO and HPBI are 6620 and 5420 cm^{-1}, respectively, and hence the intersystem crossing processes are effective for these ligands.

It is well-known in the context of lanthanide-β-diketonate complexes that ancillary ligands often play a role in terms of absorbing and transporting energy to the primary ligand β-diketone or to the central Ln^{3+} ion.[5−7] For effective energy transfer to occur, the overlap between the emission spectrum of the donor and the absorption spectrum of the acceptor is essential.[2c,27] Taking $Eu(PBI)_3(DPEPO)$ as a typical example, the possible energy migration pathways can be explained on the basis of the absorption and emission spectra of these ligands recorded at ambient and low temperature. It is evident from Figure 6 that the room-temperature emission spectrum of DPEPO is completely overlapped by the absorption spectrum of the HPBI ligand (from 300−400 nm), which implies that nearly all the radiation from the singlet state of DPEPO can be absorbed by the HPBI ligand. The singlet state of HPBI can also transfer energy to the triplet level of DPEPO (as can be noted from Figure 6, overlap between the room-temperature emission of HPBI with the low-temperature emission spectrum of $Gd(DPEPO)_3(NO_3)_3$). The singlet level of HPBI can transfer energy to the emitting level of the metal ion through its own triplet energy level (overlap between the room-temperature emission spectrum of HPBI and low-temperature emission spectrum of $Gd(PBI)_3(H_2O)_2$). The triplet level of the ancillary ligand DPEPO can also transfer energy to the central Eu^{3+} ion directly or through the triplet state of HPBI (low-temperature emission spectra of $Gd(DPEPO)_3(NO_3)_3$ and $Gd(PBI)_3(H_2O)_2$ are overlapped). Furthermore, it is clear from the room-temperature emission spectrum of **1** that transitions from the excited $^5D_1$ state to the $^7F_{0-1}$ state (538 nm, 556 nm) were also observed in addition to the $^5D_0 \rightarrow {}^7F_{0-4}$ transitions. Thus, the energy transfer process can be summarized in the four steps as shown in Figure 7.

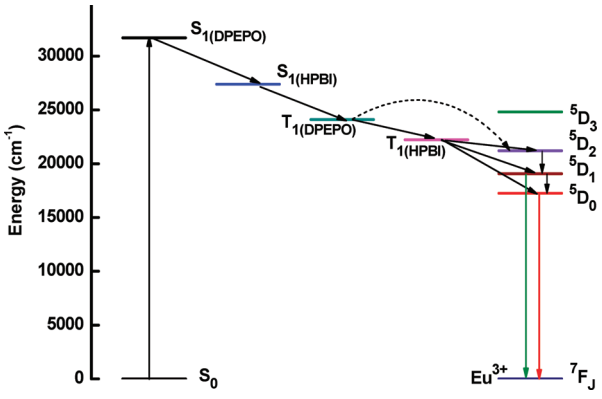

Figure 7. Schematic representation of the energy transfer mechanism for complex **1**.

Conclusions

Three new lanthanide β-diketonate complexes with bis(2-(diphenylphosphino)phenyl) ether oxide as ancillary ligand have been synthesized. The Eu^{3+} (**1**) and Tb^{3+} (**2**) complexes were structurally authenticated by single-crystal X-ray diffraction. The X-ray crystal structures of both complexes reveal a distorted square antiprismatic geometry around each Ln^{3+} ion. Detailed analysis of the single-crystal data revealed the existence of double molecular ladder structures, which are held together by $\pi-\pi$ and intermolecular hydrogen-bonding interactions. A luminescence study demonstrated that the replacement of solvent molecules of $Eu(PBI)_3(C_2H_5OH)(H_2O)$ by a chelating phosphine oxide leads to an impressive enhancement in both the overall quantum yield (from 2 to 30%) and the $^5D_0$ lifetime (from 250 to 1060 μs). Furthermore, the substantial contribution of the ancillary ligand to the overall sensitization process for Eu^{3+}-centered luminescence in $Eu(PBI)_3(DPEPO)$ is confirmed by the increase of the intrinsic quantum yield from 26 to 59% and the substantial enhancement of Φ_{sen} from 8 to 45%. By contrast, substitution of the water molecules of $Tb(PBI)_3(H_2O)_2$ by the chelating DPEPO ligand diminishes both the overall quntum yield and the $^5D_4$ lifetime values. This is due to overlap of the low energy of the ligand-centered states with the Tb^{3+}-centered excited states. Furthermore, the modest energy gap between the triplet energy level of HPBI and the emitting level $^5D_4$ (1820 cm^{-1}) facilitates the back energy transfer process. The most important result of the present work is that DPEPO can serve as an effective ancillary ligand for generating a high luminescence performance in Eu^{3+}-tris-β-diketonate complexes. As such, it is likely that such complexes will find potential applications in many photonic devices.

Acknowledgment. The authors acknowledge financial support from the Department of Science and Technology (SR/S1/IC-36/20073), University Grants Commission and the Council

of Scientific and Industrial Research, New Delhi (NWP0023). A.H.C. thanks the Robert A. Welch Foundation (F-0003) for financial support.

Supporting Information Available: TG, DSC data, X-ray crystallographic data for **2**, luminescence decay profiles, absorption and emission spectra for HPBI and DPEPO at 298 K and 77 K in CH_3CN solution. This material is available free of charge via the Internet at http://pubs.acs.org.

References

(1) (a) Brunet, E.; Juanes, O.; Rodriguez-Ubis, J. C. *Curr. Chem. Biol.* **2007**, *1*, 11–39. (b) Bünzli, J.-C. G.; Piguet, C. *Chem. Soc. Rev* **2005**, *34*, 1048–1077. (c) de Bettencourt-Dias, A. *Dalton Trans.* **2007**, 2229–2241.

(2) (a) Lehn, J.-M. *Angew. Chem., Int. Ed. Engl.* **1990**, *29*, 1304–1319. (b) de Sa, G. F.; Malta, O. L.; de Mello Donega, C.; Simas, A. M.; Longo, R. L.; Santa-Cruz, P. A.; da Silva Jr, E. F. *Coord. Chem. Rev.* **2000**, *196*, 165–195. (c) Ambili Raj, D. B.; Biju, S.; Reddy, M. L. P. *Inorg. Chem.* **2008**, *47*, 8091–8100.

(3) (a) Bellusci, A.; Barberio, G.; Crispini, A.; Ghedini, M.; La Deda, M.; Pucci, D. *Inorg. Chem.* **2005**, *44*, 1818–1825. (b) McGehee, M. D.; Bergstedt, T.; Zhang, C.; Saab, A. P.; O'Regan, M. B.; Bazan, G. C.; Srdanov, V. I.; Heeger, A. *J. Adv. Mater* **1999**, *16*, 1349–1354. (c) Fu, L.; Sa Ferreira, R. A.; Silva, N. J. O.; Fernandes, A. J.; Ribeiro-Carlo, P.; Gonalves, I. S.; de Zea Bermudez, V.; Carlos, L. D. *J. Mater. Chem* **2005**, *15*, 3117–3125. (d) Chen, X. Y.; Bretonniere, Y.; Pecaut, J.; Imbert, D.; Bunzli, J.-C. G.; Mazzanti, M. *Inorg. Chem.* **2007**, *46*, 625–637. (e) Fukuda, Y.; Nakao, A.; Hiyashi, K. *J. Chem. Soc., Dalton Trans.* **2002**, 527–533.

(4) Hasegawa, Y.; Yamamuro, M.; Wada, Y.; Kanehisa, N.; Kai, Y.; Yanagida, S. *J. Phys. Chem. A* **2003**, *107*, 1697–1702.

(5) (a) Shen, L.; Shi, M.; Li, F.; Zhang, D.; Li, X.; Shi, E.; Yi, T.; Du, Y.; Huang, C. *Inorg. Chem.* **2005**, *45*, 6188–6197. (b) Shi, M.; Li, F.; Yi, T.; Zhang, D.; Hu, H.; Huang, C. *Inorg. Chem.* **2005**, *44*, 8929–8936. (c) Xin, H.; Li, F. Y.; Shi, M.; Bian, Z. Q.; Huang, C. H. *J. Am. Chem. Soc.* **2003**, *125*, 7166–7167. (d) Xin, H.; Shi, M.; Gao, X. C.; Huang, Y. Y.; Gong, Z. L.; Nie, D. B.; Cao, H.; Bian, Z. Q.; Li, F. Y.; Huang, C. H. *J. Phys. Chem. B* **2004**, *108*, 10796–10800.

(6) (a) Pavithran, R.; Saleesh Kumar, N. S.; Biju, S.; Reddy, M. L. P.; Alves, S., Jr.; Freire, R. O. *Inorg. Chem.* **2006**, *45*, 2184–2192. (b) Pavithran, R.; Reddy, M. L. P.; Alves, S., Jr.; Freire, R. O.; Rocha, G. B.; Lima, P. P. *Eur. J. Inorg. Chem.,* **2005**, *20*, 4129–4137. (c) Biju, S.; Ambili Raj, D. B.; Reddy, M. L. P.; Kariuki, B. M. *Inorg. Chem.* **2006**, *45*, 10651–10660. (d) Biju, S.; Reddy, M. L. P.; Freire, R. O. *Inorg. Chem. Commun.* **2007**, *10*, 393–396.

(7) Xu, H.; Wang, L.-H.; Zhu, X.-H.; Yin, K.; Zhong, G.-Y.; Hou X.-Y.; Huang, W. *J. Phys. Chem. B,* **2006**, *110*, 3023–3029.

(8) (a) De Mello, C.; Wittmann, H. F.; Friend, R. H. *Adv. Mater.* **1997**, *9*, 230–232. (b) Pålsson, L.-O.; Monkman, A. P. *Adv. Mater.* **2002**, *14*, 757–758. (c) Shah, B. K.; Neckers, D. C.; Shi, J.; Forsythe, E. W.; Morton, D. *Chem. Mater.* **2006**, *18*, 603–608.

(9) Cölle, M.; Gmeiner, J.; Milius, W.; Hillebrecht, H.; Brütting, W. *Adv. Funct. Mater.* **2003**, *13*, 108–112.

(10) Eliseeva, S. V.; Kotova, O. V.; Gumy, F.; Semenov, S. N.; Kessler, V. G.; Lepnev, L. S.; Bünzli, J.-C. G.; Kuzmina, N. P. *J. Phys. Chem. A* **2008**, *112*, 3614–3626.

(11) Sheldrick, G. M. *SHELL-PC, version 5; Siemens Analytical X-ray Instruments. Inc.*: Madison, WI, U.S.A., 1994.

(12) Desiraju, G. R. *Acc. Chem. Res.* **2002**, *35*, 565–573.

(13) Roesky, H. W.; Andruh, M. *Coord. Chem. Rev.* **2003**, *236*, 91–119.

(14) Steiner, T.; Desiraju, G. R. *Chem. Commun.* **1998**, 891–892.

(15) Mascal, M. *Chem. Commun.* **1998**, 303–304.

(16) (a) Chen, J.-Q.; Cai, Y.-P.; Fang, H.-C.; Zhou, Z.-Y.; Zhan, X.-L.; Zhao, G.; Zhang, Z. *Cryst. Growth Des.* **2009**, *9*, 1605–1613. (b) Zhou, X.-X.; Cai, Y.-P.; Zhu, S.-Z.; Zhan, Q.-G.; Liu, M.-S.; Zhou, Z.-Y.; Chen, L. *Cryst. Growth Des.* **2008**, *8*, 2076–2079. (c) Cai, Y.-P.; Zhang, H.-X.; Xu, A.-W.; Su, C.-Y.; Chen, C.-L.; Liu, H.-Q.; Zhang, L.; Kang, B.-S. *J. Chem. Soc., Dalton Trans.* **2001**, *16*, 2429–2434.

(17) Jainak, C. *J. Chem. Soc., Dalton Trans.* **2000**, 3885–3896.

(18) Werts, M. H. V.; Jukes, R. T. F.; Verhoeven, J. W. *Phys. Chem. Chem. Phys.* **2002**, *4*, 1542–1548.

(19) (a) Kadjane, P.; Charbonnière, L.; Camerel, F.; Lainé, P. P.; Ziessel, R. *J. Fluoresc.* **2008**, *18*, 119–129. (b) Dejneka, M.; Snitzer, E.; Riman, R. E. *J. Lumin.* **1995**, *65*, 227–245.

(20) (a) Kai, J.; Parra, F. D.; Brito, H. F. *J. Mater. Chem.* **2008**, *18*, 4549–4554. (b) Liu, M.-S.; Yu, Q.-Y.; Cai, Y.-P.; Su, C.-Y.; Lin, X.-M.; Zhou, X.-X.; Cai, J.-W. *Cryst. Growth Des.* **2008**, *11*, 4083–4091.

(21) (a) Xiao, M.; Selvin, P. R. *J. Am. Chem. Soc.* **2001**, *123*, 7067–7073. (b) Comby, S.; Imbert, D.; Anne-Sophie, C.; Bunzli, J. C. G.; Charvonniere, L. J.; Ziessel, R. F. *Inorg. Chem.* **2004**, *43*, 7369–7379. (c) Quici, S.; Cavazzini, M.; Marzanni, G.; Accorsi, G.; Armaroli, N.; Ventura, B.; Barigelletti, F. *Inorg. Chem.* **2005**, *44*, 529–537.

(22) (a) Viswanathan, S.; de Bettenacourt-Dias, A. *Inorg. Chem.* **2006**, *45*, 10138–10146. (b) Kim, Y. H.; Baek, N. S.; Kim, H. K. *Chem. Phys. Chem.* **2006**, *7*, 213–221.

(23) (a) Sabbatini, N.; Guardigli, M.; Lehn, J.-M. *Coord. Chem. Rev.* **1993**, *123*, 201–228. (b) Nasso, I.; Bedel, S.; Galaup, C.; Picard, C. *Eur. J. Inorg. Chem.,* **2008**, 2064–2074.

(24) (a) Wrighton, M. S.; Ginley, D. S.; Morse, D. L. *J. Phys. Chem.* **1974**, *78*, 2229–2233. (b) de Mello, J. C.; Wittmann, H. F.; Friend, R. H. *Adv. Mater.* **1997**, *9*, 230–232.

(25) Latva, M.; Takalo, H.; Mukkala, V. M.; Matachescu, C.; Rodriguez-Ubis, J. C.; Kanakare, J. *J. Lumin.* **1997**, *75*, 149–169.

(26) Steemers, F. J.; Verboom, W.; Reinhoudt, D. N.; Vander Tol, E. B.; Verhoeven, J. W. *J. Am. Chem. Soc.* **1995**, *117*, 9408–9414.

(27) (a) Forster, T. Z. *Z. Naturforsch.* **1949**, *A4*, 321. (b) Berlman, I. B. *Energy Transfer Parameters of Aromatic Compounds*; Academic Press: New York, 1973.

CG900304G